Idle time selection for wire-arc additive manufacturing: A finite element-based technique

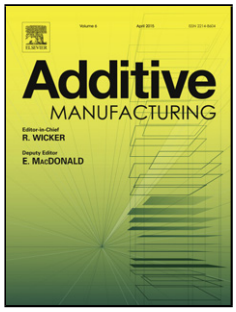

Title: Idle times selection for wire-arc-additive-manufacturing: a finite element based technique

Authors: Filippo Montevecchi, Giuseppe Venturini, Niccolò Grossi, Antonio Scippa, Gianni Campatelli

PII: S2214-8604(17)30587-0
DOI: https://doi.org/10.1016/j.addma.2018.01.007
Reference: ADDMA 272

To appear in:

Received date: 6-12-2017
Revised date: 23-1-2018
Accepted date: 27-1-2018

Please cite this article as: Filippo Montevecchi, Giuseppe Venturini, Niccolò Grossi, Antonio Scippa, Gianni Campatelli, Idle times selection for wire-arc-additive-manufacturing: a finite element based technique (2010), https://doi.org/10.1016/j.addma.2018.01.007

Title

Idle time selection for wire-arc additive manufacturing: a finite element-based technique

Authors

Filippo Montevecchi[a*], Giuseppe Venturini[a], Niccolò Grossi[a], Antonio Scippa[a], Gianni Campatelli[a]

[a] *Affiliation:* Department of Industrial Engineering, University of Firenze, Via di Santa Marta 3, Firenze, 50139, Italy.

[*]*Corresponding author: Tel.*: +39-055-2758726. *E-mail address*: filippo.montevecchi@unifi.it.

Abstract

Wire-arc additive manufacturing is a metal additive manufacturing process that enables the production of large components at a high deposition rate. This process transfers a large amount of heat to the workpiece, requiring the introduction of idle times between the deposition of subsequent layers so that the workpiece cools down. This procedure prevents the workpiece from collapsing and ensures a suitable interpass temperature. The main challenge is the selection of such an idle time capable of ensuring the required interpass temperature, because the cooling rate of the workpiece changes throughout the process, entailing the need for a different idle time between the deposition of subsequent layers to achieve a constant interpass temperature.

This paper proposes an innovative approach to schedule the deposition of interlayer idle times for wire-arc additive manufacturing process. The technique is based on a finite element analysis of the thermal behavior of the workpiece, by solving the heat transfer equations. The simulation data are processed using the developed algorithm to compute specific idle times for the deposition of each layer, thereby ensuring a constant interpass temperature. The effectiveness of the proposed technique is validated by experiments performed on a test case component. The idle times are calculated using the proposed technique, by simulating the process, and used to manufacture the test case. The temperature data measured during the process are compared with the FE simulation results to verify the accuracy of the model. An analysis of the geometry of the manufactured workpiece confirms that the adoption of the idle times obtained by the proposed technique prevents the occurrence of major structural collapses.

Keywords

Wire-Arc Additive Manufacturing, Gas-Metal-Arc-Welding, Finite Element.

1. Introduction

The wire-arc additive manufacturing (WAAM) process is an additive manufacturing (AM) technology to produce metal components. This process produces the components by the selective deposition of subsequent layers using an arc welding heat source to melt a wire feedstock. Standard arc welding equipment can be used to perform WAAM operations, using different technologies [1], such as gas metal arc welding (GMAW), gas tungsten arc welding (GTAW), or plasma arc welding (PAW). Compared to other metal AM processes, the main advantages of WAAM are the high achievable deposition rate and the efficiency in manufacturing large components[2].

However, the components manufactured using WAAM are prone to thermal issues caused by the large amount of heat introduced in the workpiece during the process [3], which could lead to excessive residual stresses, significant distortions [4], and workpiece structural collapse [5]. A common practice to mitigate such issues is the introduction of idle times between the deposition of subsequent layers [6], during which the workpiece cools down transferring the accumulated heat to the environment. Hence, the idle time value controls the interpass temperature, namely the

temperature of the workpiece at the beginning of the deposition of subsequent layers. This parameter is crucial for the WAAM process: Zhao et al. [7] showed that by increasing the idle times (i.e., by decreasing the interpass temperature), the magnitude of the residual stresses can be reduced; Geng et al. [8] stated that controlling the interpass temperature is essential to avoid bead defects and to prevent component collapse. Moreover, the interpass temperature selection is fundamental to avoid solidification defects and to achieve adequate material properties. Shen et al. [9,10] investigated the influence of interpass temperature on the WAAM processing of iron aluminide alloys, concluding that it has a significant influence on the yield stress, elongation, and the occurrence of longitudinal cracking. Ma et al. [11] studied titanium aluminide alloys and found a significant influence of interpass temperature on the local chemical composition, microstructure, phase concentration, and microhardness.

Currently, two main techniques are used to schedule the idle times in WAAM processes: (i) fixed idle time selection and (ii) substrate temperature monitoring. In the first case, a fixed idle time is introduced at the end of the deposition of each layer in the deposition part program [12]. This technique allows the workpiece to cool down; however, it requires a series of pretests to set the correct idle time. Furthermore, fixed idle times might not allow to maintain a constant interpass temperature. This is due to the heat transfer mechanism from the molten pool to the workpiece. As shown by Zhao et al. [13], the most relevant heat flux is the conduction in the building direction, which is significantly affected by the workpiece height, i.e., by the number of formerly deposited layers. Therefore, to provide the same interpass temperature, the idle time should be increased as the deposition progresses.

This is usually achieved by the second technique, i.e., monitoring the substrate temperature by using a sensor, usually a thermocouple. After the deposition of a layer, the process is kept idle until the thermocouple signal reaches the prescribed value. Despite that this technique keeps the substrate temperature constant at the end of the deposition of each layer, it does not allow to achieve a constant molten pool size. Indeed, with the increase in the distance between the current layer location and the substrate, the volume of molten pool increases, as shown by Wang et al. [14]. Similar to that in the fixed idle, this is related to the decrease in the conductive heat flux due to the increase in workpiece height during the deposition process. This is a significant drawback of the substrate temperature monitoring technique, because limiting the increase in the molten pool volume is crucial to achieve adequate process results, both in terms of homogeneous mechanical properties [14,15] and avoiding the local structural collapse of the workpiece that result in poor dimensional accuracy [16].

This paper proposes an innovative technique to schedule the interlayer idle times for the WAAM technology, based on a finite element (FE) simulation of the process. The interpass temperature is monitored during the simulation at different points for each layer. A different idle time is calculated for the deposition of each layer, ensuring a constant interpass temperature on the previously deposited layer. It is demonstrated that this approach ensures a constant molten pool size during the process. The calculated idle times can be included as dwells in the WAAM part program, ensuring the consistency between the simulated and the actual process. The usage of a FE simulation rather than a sensor-based monitoring has a twofold advantage: it overcomes the issues related to temperature measurements in the workpiece areas close to the molten pool [17] and enables to perform sensitivity analysis using different interpass temperatures. To verify its effectiveness, the proposed technique was used to schedule the idle times for the manufacturing of a test case component. Such component was then manufactured using the prescribed idle times. Finally, coordinate measurement machine (CMM) measurements were made on the workpiece to verify the effect of the proposed approach on the dimensional accuracy of the component.

Section 2 shows the details of the proposed idle time calculation technique, and section 3 presents the test case manufacturing procedure and the experimental results.

2. Proposed technique

This paper proposes a novel approach to calculate the idle times required to achieve a constant interpass temperature and to ensure a constant molten pool size in WAAM operations. The basic idea is to monitor the cooling of each layer right after its deposition using a FE simulation of the WAAM process, calculating the required idle times to meet the predefined interpass temperature. Unlike the most common procedure of monitoring the substrate temperature in a set of fixed points, in this technique, a specific control point is associated with each layer. This enables a local control of the interpass temperature, compensating the reduction of the conductive heat flux. The FE simulation, a consolidated practice for WAAM [18] and different metal AM processes [19], provides the knowledge of the workpiece temperature field in an arbitrary point, an outcome barely achievable by direct measurement [20].
This section presents the two key points of the proposed technique:

- FE modelling of the WAAM process.
- The idle time computation algorithm.

2.1 FE modelling of the WAAM process

In the proposed technique, a numerical simulation is used to evaluate the thermal behavior of the workpiece. The WAAM process is simulated at a macroscale level, i.e., solving the heat transfer problem in the workpiece. For simplification, the heat and mass transfer phenomena, which occur in the molten pool, are neglected. This is a common approach in the simulation of many metal AM processes [21]. The problem is described by the partial differential equation of heat diffusion in a solid body, as shown in Eq. 1:

$$\nabla\big(\lambda(T)\nabla T(X,Y,Z,t)\big) + q(X,Y,Z,t) = \rho C_p(T)\frac{\partial T(X,Y,Z,t)}{\partial t} \qquad \text{Eq. 1}$$

where T is the unknown temperature, a function of time (t) and position (X,Y,Z); $\lambda(T)$ is the temperature-dependent thermal conductivity; $C_p(T)$ is the temperature-dependent heat capacity; ρ is the mass density; and $q(X,Y,Z,t)$ is the source term of the equation, representing the heat input of the welding process. The final term is a function of both time and spatial coordinates, because it is related to the deposition path. The boundary and initial conditions of Eq. 1 are presented in Eq. 2:

$$\begin{cases} -\lambda(T)\dfrac{\partial T}{\partial \vec{n}}\Big|_{\Omega,t} = h(T - T_\infty) \\ -\lambda(T)\dfrac{\partial T}{\partial \vec{n}}\Big|_{\Omega,t} = \varepsilon\sigma(T^4 - T_\infty^4) \\ T|_{x,y,z,0} = T_0 \end{cases} \qquad \text{Eq. 2}$$

The first relation represents the boundary condition of convection described by Newton's law, where h is the heat transfer coefficient, T_∞ is the far-field air temperature, and $\vec{n}$ is the normal vector of the heat transfer surface Ω. The second relation represents the boundary condition of radiation to the environment, described by the Stefan-Boltzmann law, where ε is the surface emissivity and σ is the Stefan-Boltzmann constant. The third relation represents the initial condition of uniform temperature (T_0) throughout the integration domain.
Eq. 1 is solved using the FE method, according to the techniques previously presented in [22,23]. The most distinctive features of the simulation technique presented in this study are as follows:

- The heat source model
- The material deposition modelling

2.1.1 Heat source model

The heat source included in the simulation delivers the heat input of the welding process to the workpiece. The WAAM process involves complex interactions among the electric arc, feedstock, and molten pool, which occur at different dimensional and time scales [24]. To increase the time efficiency of the simulation, a heat source model is used.
One of the most widespread model of heat source for the arc welding processes is the double ellipsoid one, proposed by Goldak et al. [25]. In the Goldak model, the heat input is the heat generated internally per unit volume (W/m^3), having a Gaussian distribution in a coordinate system moving along the deposition path. The heat source model used in this paper is a modified version of the double ellipsoid one [22], tailored for the GMAW process. The heat distribution function is presented in Eq. 3:

$$\dot{q} = \begin{cases} \dot{q}_b = \frac{6\sqrt{3}\dot{Q}_b f_{f,r}}{\pi\sqrt{\pi} a_{f,r} bc} \exp\left[-3\left(\frac{x^2}{a_{f,r}^2} + \frac{y^2}{b^2} + \frac{z^2}{c^2}\right)\right] \\ \dot{q}_w = \frac{\dot{Q}_w}{V_{el}} \end{cases} \quad \text{Eq. 3}$$

In the proposed heat source, the heat input of the welding process is split into two power density contributions: the base metal ($\dot{q}_b$) and the filler or deposited metal ($\dot{q}_w$). This strategy allows to control the amount of power transferred to both the base ($\dot{Q}_b$) and the filler metal $\dot{Q}_w$, provided that the following condition is fulfilled:

$$\dot{Q}_b + \dot{Q}_w = \dot{Q} = iV\eta \quad \text{Eq. 4}$$

That is, the sum of the base and filler metal power must be equal to the total power transmitted to the workpiece ($\dot{Q}$), calculated as the product of the welding current *i*, the welding voltage *V,* and the arc efficiency factor η.
The power delivered to the base metal is distributed according to a Gaussian function as in the double ellipsoid model. Eq. 3 depicts the power density function of the base metal. The terms *x*, *y,* and *z* are the point coordinates in the moving frame of reference *O* as shown in Figure 1b (local coordinates): the *x* axis is directed along the feed direction, the *z* axis is directed in the arc aiming direction outward from the molten pool, and the y axis is determined by the right hand rule. The local coordinates of a generic node depend on its global coordinates (*X, Y, Z*) and on the simulation time, namely on the toolpath.

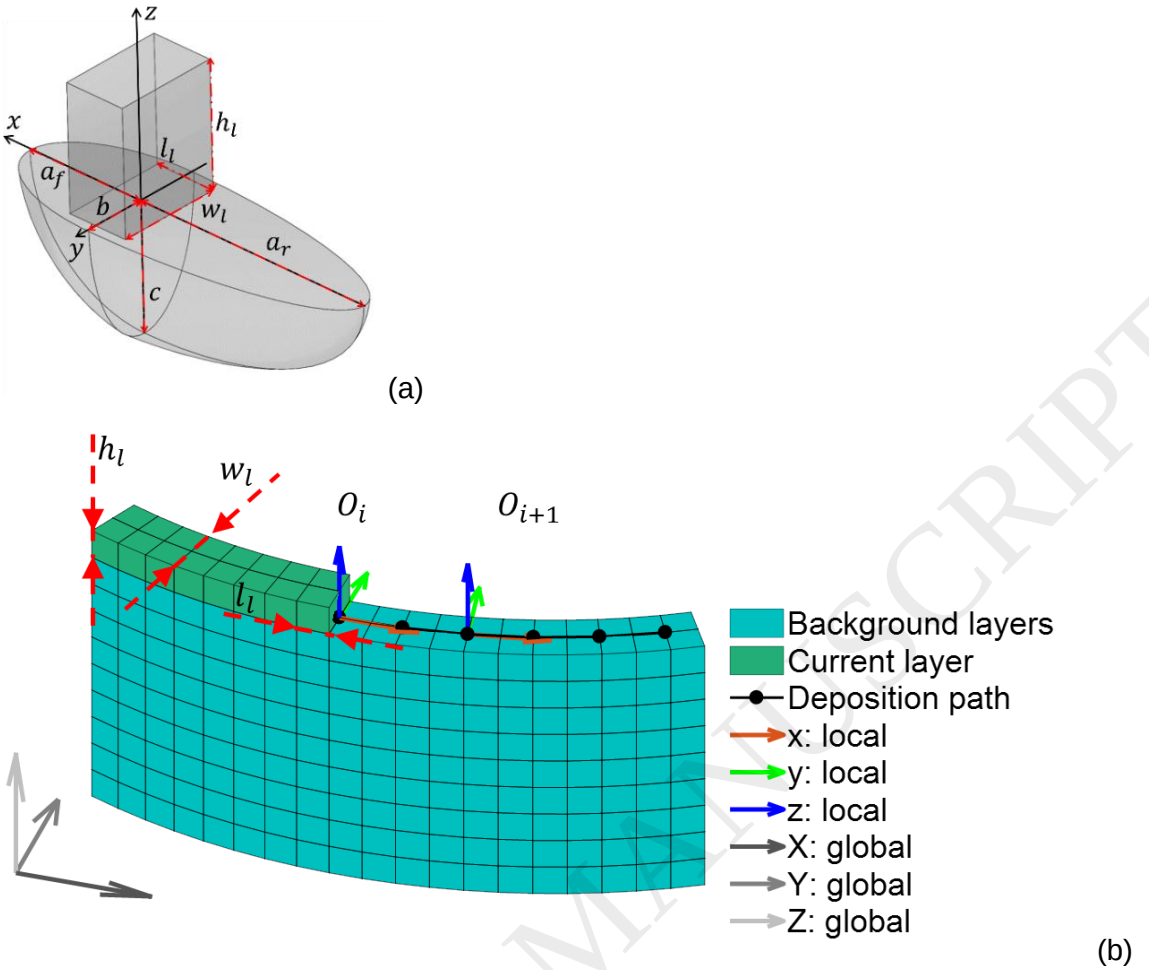

Figure 1: Heat source model used for WAAM simulation (a); Moving coordinate system used in the heat source definition (b).

The terms a_f, a_r, b, and c are the shape factors of the base metal distribution, i.e., the semi-axes of a double ellipsoidal surface as shown in Figure 1a. The subscripts *f* and *r* represent the front and the rear parts of the ellipsoids, respectively. If a point is located at a positive *x* coordinate, the a_f value will be used for the *x* semi-axis. By contrast, a_r will be used for negative *x* values. The terms f_f and f_r are the distribution factors, giving the power repartition between the front and back sides of the ellipsoid.

For the filler metal, the heat source model uses a constant power density distribution. As depicted in Eq. 3, the power density $\dot{q}_w$ is calculated by dividing the deposited metal power $\dot{Q}_w$ by V_{el}, the volume of the elements lying inside a box-shaped control volume (Figure 1a), moving along the deposition path. The dimensions of such control volume l_l, w_l, and h_l are related to the mesh size of the deposited material, as shown in Figure 1b. Further details on the adopted heat source model, including the control volume parameters, are provided in [22].

2.1.2 Material deposition modelling

In every AM process, the workpiece is manufactured by progressive material addition. This material deposition process is simulated using specific techniques. This paper uses a technique described in the welding simulation literature [26], based on inactive element strategy [27]. In this technique, all the elements representing the workpiece are included from the beginning of the simulation, as shown in Figure 2a. The progressive addition of a material is simulated by modifying the value of its thermal conductivity: at the initial state, an extremely low value is assigned to the

thermal conductivity of the elements representing the weld layers, and then, it is increased to its actual value when the element temperature exceeds a threshold value. This technique is effective in simulating the material deposition because the low thermal conductivity of the inactive elements does not allow any heat transfer between the active and inactive elements, making the contribution of the former ones negligible to the thermal behavior of the base material. Moreover, the inactive elements experience a significant temperature increase only when they are directly heated by the heat source, making the activation sequence consistent with the actual deposition process.
The presented technique is implemented in the FE solver using Eq. 5 to define the material thermal conductivity:

$$\lambda(T(\tau)) = \gamma(T_{max})\lambda_{act}\big(T(\tau)\big) + \big(1 - \gamma(T_{max})\big)\lambda_{quiet} \quad \text{Eq. 5}$$

where λ is the thermal conductivity, which is a function of the temperature T at the current simulation time τ; λ_{act} and λ_{quiet} are the active and inactive values of the thermal conductivity; γ is the activation variable, which is a function of T_{max}, i.e., the maximum temperature experienced by the element up to the current simulation time. The pattern of $\gamma(T_{max})$ is shown in Figure 2b: the activation is performed in a temperature range to avoid convergence issues in the FE simulation.

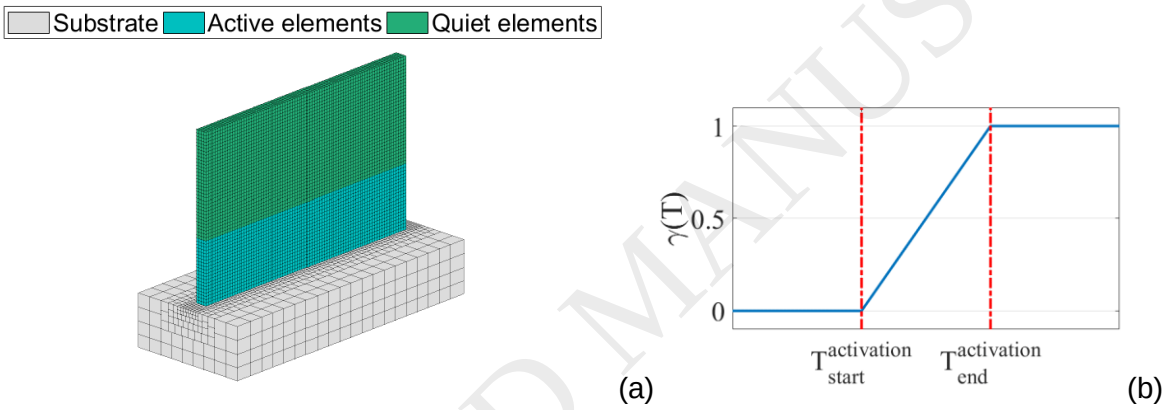

Figure 2: Active and inactive elements on a sample workpiece (a) and the function used for the element activation (b).

It must be pointed out that the element temperature is evaluated at its integration points; Eq. 5 is hence evaluated for every time step at every integration point of the deposited material elements. Therefore, the activation of an element is completed when γ is equal to 1 at all the integration points.

2.2 Idle time calculation

The FE simulation technique presented in section 2.1 is used to predict the thermal behavior of the workpiece during the WAAM process. This section depicts how the process model is used to calculate the idle times for the deposition of interlayers.

The proposed approach consists of the following steps, which is repeated for the deposition of each layer of the component:

- The deposition of the current layer is simulated without any idle time at the end of the calculation.
- The final temperature field at the end of the simulation is prescribed as the initial condition to a twin FE model of the workpiece. Then, the natural cooling of the workpiece for a fixed

period of time is simulated, which is significantly higher than the time expected to meet the required interpass temperature constraint.

- The temperature time history of a predetermined node, serving as a specific monitoring point for the current layer, is extracted from the cooling simulation results. Such data are analyzed, thereby calculating the idle time associated with the deposition of the current layer.
- At this stage, the deposition of the next layer is simulated, prescribing an initial idle time equal to the calculated one.

The following subsections provide a detailed description of the key aspects of the proposed technique: the control point positioning, the deposition and cooling simulation steps, and the idle time calculation.

2.2.1 Control node positioning

A control point is defined for each layer of the workpiece to monitor its cooling after the deposition and to calculate the required idle time to meet the target interpass temperature. In the simulation domain, the control points correspond to a set of FE nodes, located on the top surface of each layer at the end of its deposition path, i.e., the points of the deposition path where the idle time shall be introduced. Figure 3 shows this arrangement on a straight wall, which is used as the sample component.

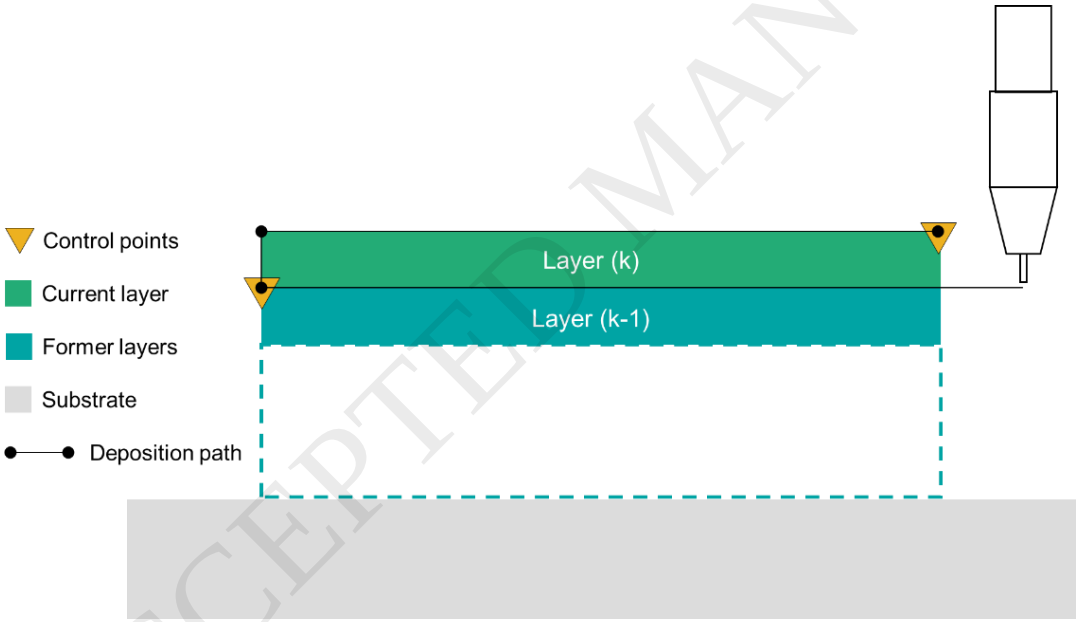

Figure 3: Control point location strategy.

In this case, the deposition is carried out following an alternate strategy, i.e., the deposition end points of subsequent layers (circle marks) lying on the opposite ends of the wall, resulting in an alternate positioning of the control nodes. The selection of the end of each layer as the control point is a conservative strategy because it is the point that will experience the highest temperature after the deposition. Therefore, compared to other areas of the layer, it requires the highest idle time to achieve the target interpass temperature.

2.2.2 Deposition and cooling simulation

In this paper, a specific idle time for each layer is calculated to fulfill the constant interpass temperature condition. The required cooling time is dependent on the amount of heat accumulated in the workpiece during the deposition and cooling phases of the former layers. Therefore, the idle time for the deposition of each layer cannot be identified separately: the calculation for a layer must consider the results of the former ones, which is achieved in this paper by using the simulation strategy outlined in Figure 4.

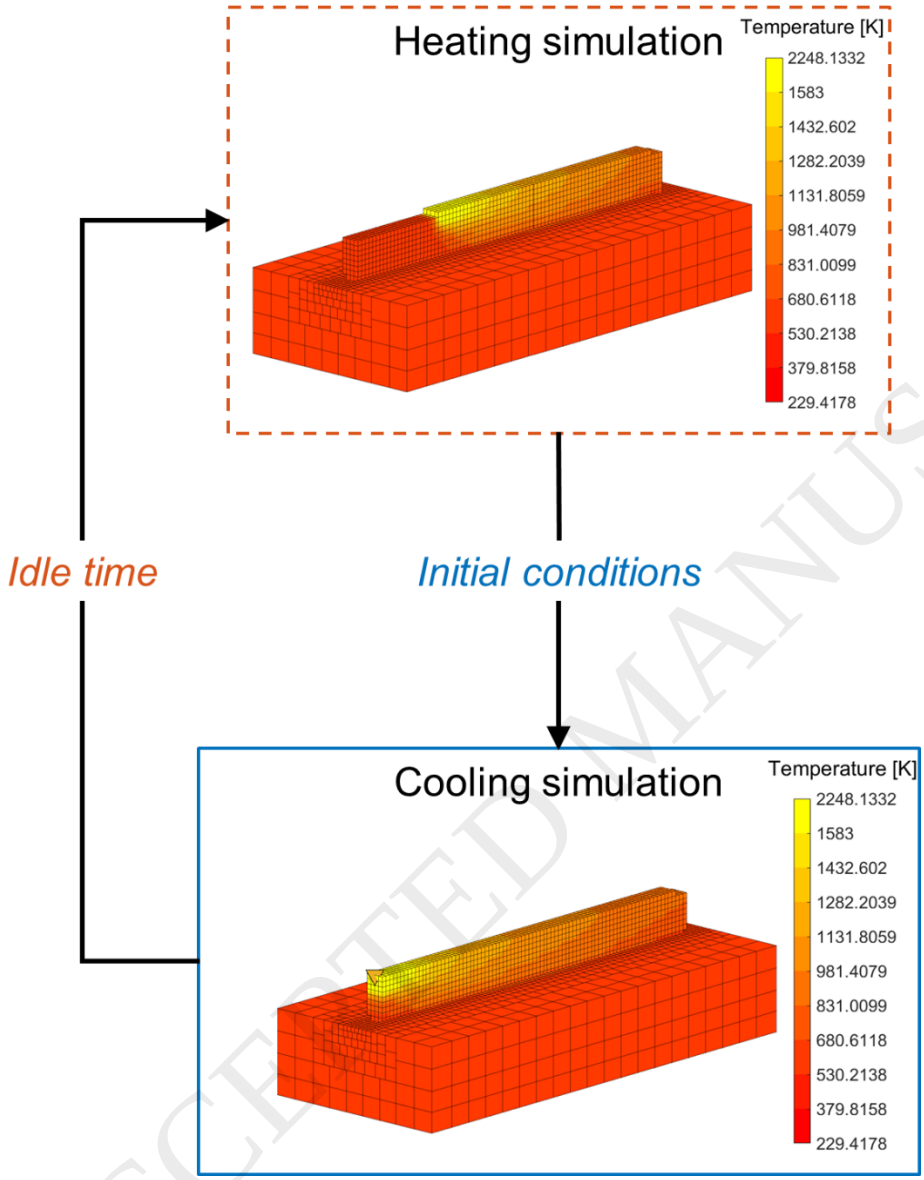

Figure 4: FE simulation strategy used for the idle time calculation

The technique is based on twin models, one for the heating (deposition) and one for the cooling simulation. The two models are identical in terms of mesh topology, material properties, and boundary conditions, and the only difference is the heat source, which is used only in the heating model. In the heating step, the deposition of the current layer is simulated without any idle time at the end of it. The end state of this simulation is used to define the initial conditions for the cooling step, i.e., the initial temperature field and the active/inactive state of the elements. The initial element activation state is prescribed by the initial value of the $\gamma(T_{max})$ variable. The cooling simulation is then started, reproducing the thermal behavior of the workpiece during the idle time at the end of the deposition of the current layer. To ensure that the control node of the current layer reaches the required interpass temperature, the cooling behavior must be simulated for a longer

time than the expected idle time. This is achieved by tuning the total simulation time for the specific workpiece and process parameters. It must be pointed out that this is not a time-consuming approach because a large time step can be used in the cooling phase.
The results of the cooling simulation are used to calculate the idle time required for the current layer to reach the desired interpass temperature. The computed idle time is then used as input for the heating simulation of the new layer. This is achieved by including an initial idle time in the heating simulation of the generic layer *k*, corresponding to the value calculated for layer *k-1*. This strategy allows to consider the effect of the former idle times.
The proposed idle time calculation technique was implemented using a MATLAB code to start the FE simulations, update the models, and calculate the idle times. The FE simulation can be implemented using any commercial FE code that is suitable to deal with nonlinear heat transfer analyses. In this paper, the commercial FE code LS-DYNA is used. The heat source model and the element activation techniques, described in section 2.1.1, are implemented using the *LOAD_HEAT_GENERATION and the *MAT_THERMAL_USER_DEFINED features, respectively [28].

2.2.3 Idle time calculation

The idle time calculation procedure is outlined in Figure 5.

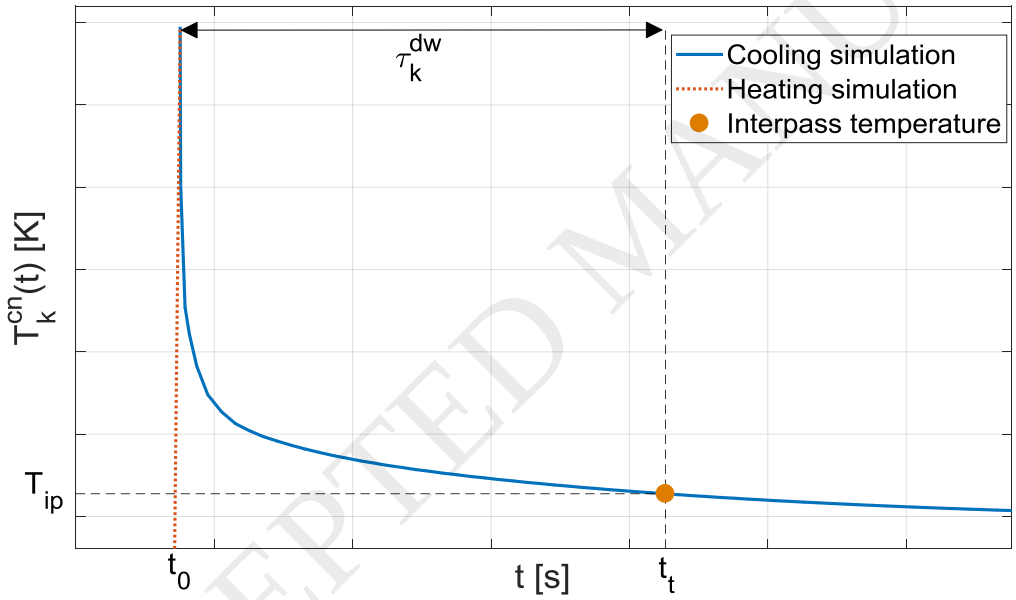

Figure 5: Idle time calculation procedure.

Let T_k^{cn} be the time history of the control node temperature returned by the FE solver during the cooling simulation of the *k*-th layer. These data can be expressed as a continuous function of the simulation time (t) by a piecewise linear interpolation of the discrete data. This step returns the function $T_k^{cn}(t)$. Let T_{ip} be the target interpass temperature. The goal is to identify the target simulation time t_t, which fulfills the following equation:

$$T_k^{cn}(t_t) - T_{ip} = 0 \qquad \text{Eq. 6}$$

Eq. 6 can be solved using numerical techniques. This solution is directly used to calculate the idle time corresponding to the *k*-th layer, τ_k^{dw}:

$$\tau_k^{dw} = t_t - t_0 \quad \text{Eq. 7}$$

where the term t_0 corresponds to the initial time value of the *k*-th layer cooling simulation. Hence, at the end of the calculation, an idle time value is associated with each layer.

3. Verification of the proposed technique

The proposed technique was applied on a test case component, and the idle times required for the manufacturing process were identified. The manufacturing process was then simulated using the calculated idle times. Simulation data were postprocessed to evaluate the trend of the molten pool size with the increase in the number of layers deposited, thus assessing the fulfillment of the activity goal.
The test case was manufactured using a WAAM machine. A thermocouple was attached to the substrate of the component to acquire the temperature time history of a specific point during the process. These data were compared with those of FE simulation to show the accuracy of the modelling techniques used in this paper. After the test case was manufactured, its geometry was measured using a CMM and compared with the reference geometry, and the results showed that no significant collapses occurred with the use of the proposed idle time calculation scheme.

3.1 Test case and experimental description

The test case used in this paper is an airfoil. The schematic and dimensions of the component are shown in Figure 6a: the cross-section is constant throughout the chordal length, and the camber line geometry is defined according to the NACA 9403 designation. The deposition was carried out using a 0.8-mm wire made of ER70S-6, and a standard filler material was used for carbon steel welding. The airfoil was deposited on a block made of S235JR structural steel with low carbon content. The manufactured test case is shown in Figure 6b.

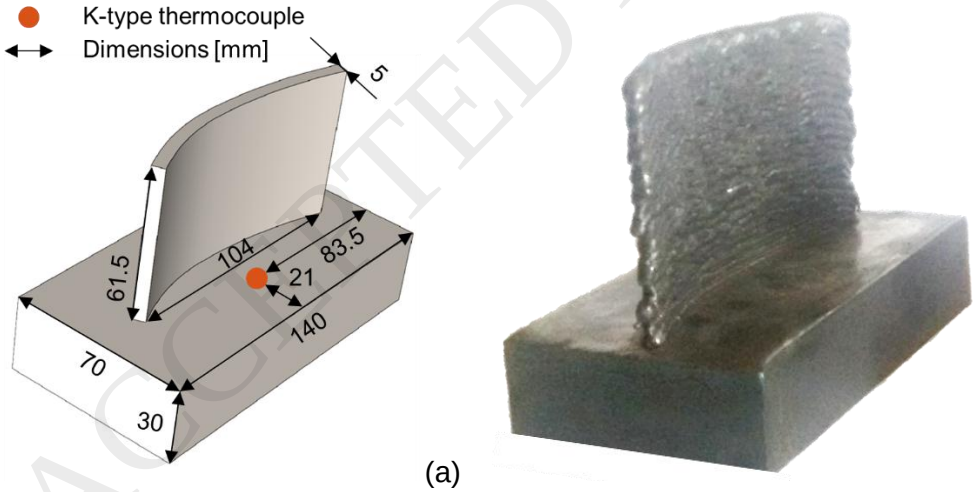

(a) (b)

Figure 6: The airfoil used as test case: dimensions and thermocouple arrangement (a); actual manufactured part

The WAAM process was carried out using a commercial GMAW machine (AWELCO 250 PULSEMIG), installed on a three-axis milling machine. The process parameters used for the deposition are listed in Table 1.

Table 1: Process parameters used for the test case manufacturing.

Current [A]	Voltage [V]	Heat input [W]	Deposition	Wire feed speed

			speed [mm/min]	[m/min]
80	18	1440	300	4.6

A layer of about 1.5-mm height and 5.0-mm width was obtained using the presented parameters, thus requiring 41 layers to create the geometry. No preheating was applied to the substrate, starting the deposition at room temperature. A k-type thermocouple was used to measure the substrate temperature during the manufacturing process. The sensor was attached to the top surface of the substrate positioned as shown in Figure 6a. The thermocouple signal was logged using a National Instrument 9213 acquisition system at a sample rate of 10 Hz. After the deposition process, the workpiece was scanned using a Mitutoyo Euro Apex C776 CMM to acquire its geometry.

3.2 FE model and idle time calculation

The FE model of the test case was developed using 24543 hexahedral elements with a single integration point. The resulting FE model is shown in Figure 7.

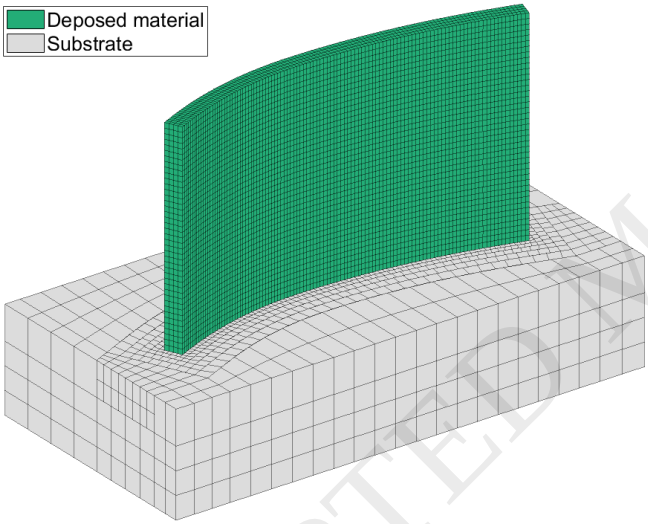

Figure 7: FE model of the test case.

The FE simulations were carried out using the FE solver LS-DYNA, using a Crank-Nicolson time integration scheme with a variable time-stepping algorithm [28] that adapted the time step size to achieve a maximum temperature variation of 400 K per step. Temperature dependency was considered for both the thermal conductivity and the heat capacity using literature curves [29]. The thermal conductivity was artificially increased in the liquid range to capture the convective heat transfer in the molten pool [30]. The inactive value of the thermal conductivity was set as a fraction (1.0e-5) of its active state value, according to the recommendations of Michaleris [26]. The latent heat of fusion was considered for both the base and the deposited materials using the technique presented in [22,23]. The latent heat values together with the solidus and liquidus temperatures of both ER70S-6 and S235JR were obtained from the literature [31,32]. Both free convection and radiation were included in the FE model. The convective coefficients were calculated by nondimensional correlations commonly used in the heat transfer literature [33]: 9.94 W/m^{2}K on the substrate vertical surfaces, 10.44 W/m^{2}K on the substrate top surface, 5.22 W/m^{2}K on the substrate bottom surface, and 7.8 W/m^{2}K on the airfoil vertical surfaces. The far-field temperature

was set to 294 K, equal to the room temperature. For the radiation condition, the emissivity was set to 0.4, according to the literature data [34].
First, the FE model of the test case was used to calculate the interlayer idle times, prescribing a constant interpass temperature of 600 K [29]. The result of this calculation is shown in Figure 8a, where the idle times are presented as a function of index of the current layer. As expected, the proposed technique prescribes a significant increase in the idle time to achieve a constant interpass temperature on the top of the current layer, thus compensating the reduction of the conductive heat flux in the substrate direction. Besides, the idle time increase is not constant with the workpiece growth. The curve shows a sigmoidal trend with three distinct regions (Figure 8a) having different rates of idle time increase. Such pattern can occur considering the distance between the substrate and the molten pool. The vicinity region corresponds to the first layers, where the substrate is close to the molten pool. This creates a heat sink effect leading to a quick cooling. In this phase, the growth of the workpiece has a marginal effect on the conductive heat flux, resulting in the small variations of the idle time. However, the high substrate distance region corresponds to the last layers, where the heat sink effect of the substrate is significantly reduced. In this condition, the cooling problem approaches the one-dimensional behavior, where the magnitude of the conductive heat flux is roughly proportional to the overall workpiece height. Therefore, the conductive heat flux experiences a slight reduction for any additional layer, because of the lower value of the layer height than the workpiece height, resulting in a slight increase in the idle times. Considering these results, the central part of the curve is labeled as a transition region, in which the heat sink effect of the substrate on the cooling behavior is reduced, resulting in a high increase in the idle times. It must be pointed out that the extensions of the three regions are expected to be dependent on the prescribed interpass temperature, process parameters, and workpiece geometry.

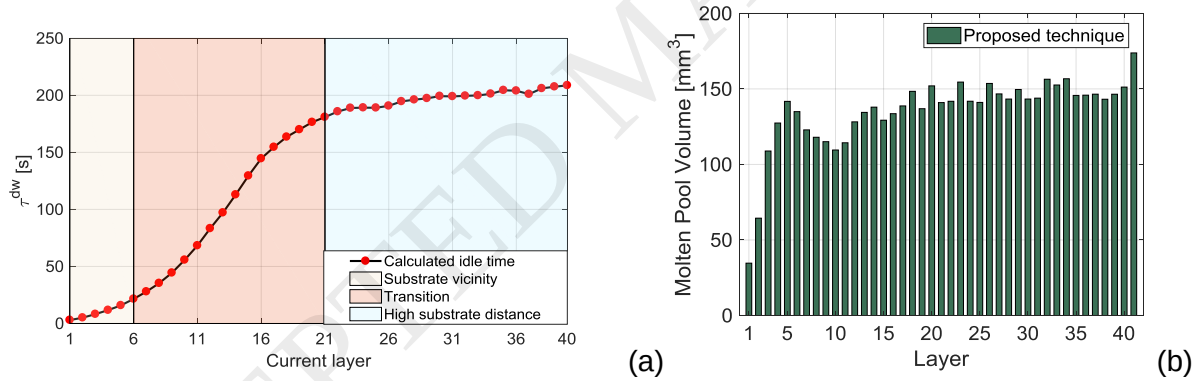

Figure 8: Results of the idle time calculation procedure: idle time values (a) and molten pool volume for each layer.

After the calculation of the idle times, the manufacturing of the whole test case was simulated including the idle times to evaluate the effect on the molten pool size, quantified as volume of the elements above the solidus temperature [35]. The calculation was repeated for each step of the simulation results, and an average value was extracted for each layer. The result of this calculation is shown in Figure 8b. It is highlighted that the molten pool size is almost constant throughout all the layers. Indeed, except for the initial six layers, the maximum variation of the molten pool volume is below 15%. The initial steep growth of the molten pool is related both to the absence of preheating and to the heat sink effect of the substrate. This is consistent with the trend of Figure 8a, which shows that the upper bound of the substrate vicinity region is in correspondence of the sixth layer. It is expected that preheating of the workpiece would result in a slighter variation in the molten pool volume in the first layers.

3.3 Experimental results

This section presents and discusses the results of both thermocouple and CMM measurements. The goal of the thermocouple measurements was to highlight the accuracy of the FE simulation technique. Figure 9 shows the comparison of the thermocouple data with the temperature time history of a node located in the same position. The thermal history of the first 17 layers was corrupted by excessive measurement noise. Therefore, in Figure 9, we show the numerical-experimental comparison starting from the 18th layer. However, this does not affect the relevance of the comparison because as already mentioned, the thermal history of each layer is considerably affected by the former ones. Hence, a good correlation of the simulated and measured data in the top layers highlights a good correlation over the whole manufacturing cycle.

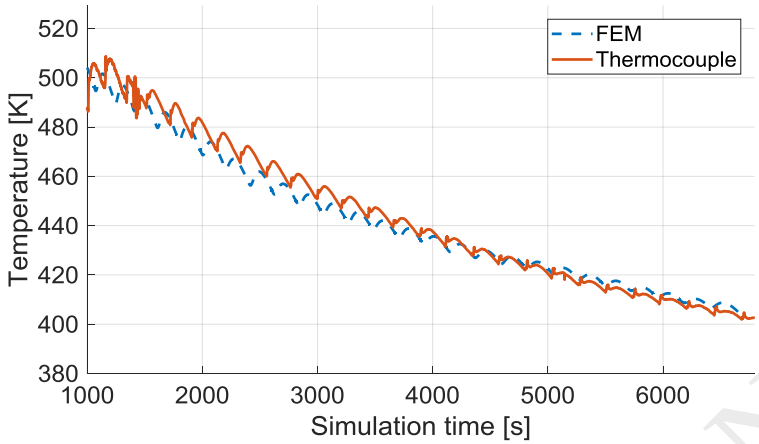

Figure 9: Comparison of simulation and thermocouple data.

Figure 9 shows that the simulation data are in good agreement with the measured ones in terms of both overall trend and specific values. This is a relevant result because the proposed idle time calculation is effective only if the FE model accurately predicts the workpiece temperature field; otherwise, the interpass temperature constraint might not be fulfilled in the actual process. Moreover, this result supports the reliability of the molten pool size pattern shown in Figure 8b, which was obtained from the simulation data.

The goal of the CMM measurements was to show that the proposed technique allowed to avoid major part collapses without performing trial-and-error operations to select the idle times. The functional surfaces of the airfoil, namely the pressure and the suction side, were scanned by the CMM and compared with the target surfaces, as shown in Figure 10.

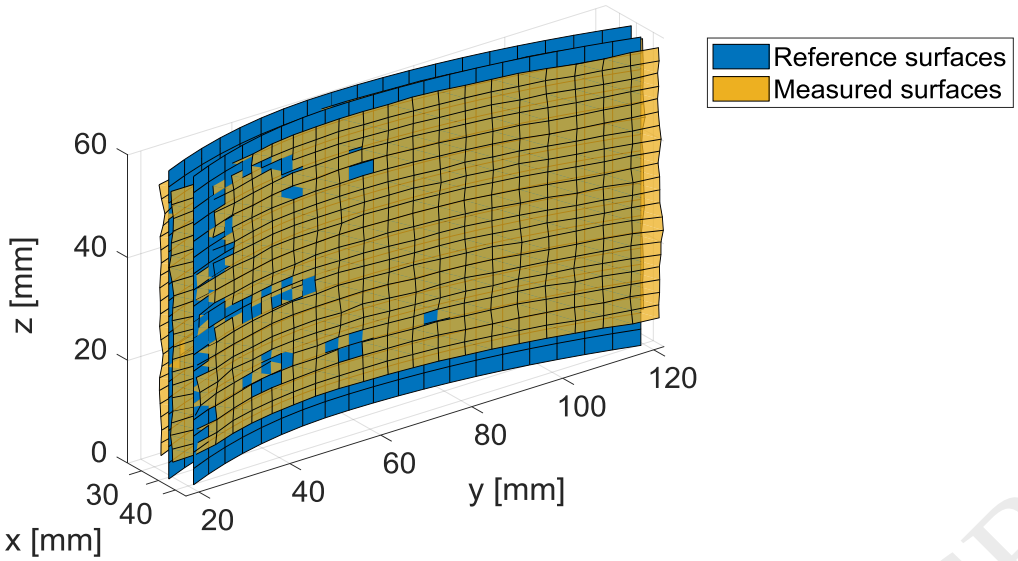

Figure 10: Comparison of the measured blade surface and the reference CAD model.

The average deviation from the target surface was 0.65 mm for the pressure side and 0.39 mm for the suction side. It must be pointed out that the measured surfaces were affected by a significant waviness (Figure 6b) typical of the WAAM process [36]. This result confirms that no significant collapse occurred during the deposition process. However, it is worthwhile to highlight that despite the effectiveness of the proposed technique, an excessive interpass temperature could still collapse the workpiece. Therefore, it is important to refer to the literature that provides the interpass temperature values for various materials.

4. Conclusions

This paper presents a novel approach to calculate the interlayer idle times required for WAAM operations. The proposed technique uses a FE model to simulate the thermal behavior of the workpiece during the process. This enables the calculation of suitable idle times. The proposed algorithm calculates an idle time value specific for each layer allowing to meet the condition of constant interpass temperature. Such parameter is measured by observing the top surface of the current layer. This allows to limit the increase in the molten pool size during the deposition process responsible for component collapses and nonhomogeneous mechanical properties along the building direction.

The effectiveness of the proposed technique was tested on a test case component. The idle times were calculated according to the proposed technique, which can be used in the manufacturing process. The deposition was then simulated using the calculated idle time. An analysis of the simulation results confirms that in the selected test case, the proposed technique effectively ensures a constant molten pool size. The test case, using the calculated idle times, was monitored using a thermocouple installed on the substrate. The measured data were compared with the simulation time histories, thereby proving the accuracy of the FE model in predicting the thermal behavior of the WAAM workpiece and, hence, in calculating suitable idle times. Finally, the geometry of the manufactured test case was acquired and compared with the reference CAD model. This comparison confirmed that no major collapses occurred by the use of the proposed technique, because the deviation between the reference and measured geometries was within the range of the component surface waviness.

In conclusion, the proposed technique achieves two significant goals: it provides a constant interpass temperature and ensures a constant molten pool size. Moreover, the use of an FE model avoids time-consuming trial-and-error procedures to select the idle times, thus providing a simulation tool to investigate the effect of process parameters and toolpath on the idle times. This can contribute to increase the performance of the WAAM process both in terms of quality and productivity.

References

[1] K.F. Ayarkwa, S.W. Williams, J. Ding, Assessing the effect of TIG alternating current time cycle on aluminium wire + arc additive manufacture, Addit. Manuf. 18 (2017) 186–193. doi:10.1016/j.addma.2017.10.005.

[2] C. V Haden, G. Zeng, F.M. Carter, C. Ruhl, B.A. Krick, D.G. Harlow, Wire and arc additive manufactured steel: Tensile and wear properties, Addit. Manuf. 16 (2017) 115–123. doi:10.1016/j.addma.2017.05.010.

[3] W.E. Frazier, Metal additive manufacturing: A review, J. Mater. Eng. Perform. 23 (2014) 1917–1928. doi:10.1007/s11665-014-0958-z.

[4] B.A. Szost, S. Terzi, F. Martina, D. Boisselier, A. Prytuliak, T. Pirling, M. Hofmann, D.J. Jarvis, A comparative study of additive manufacturing techniques: Residual stress and microstructural analysis of CLAD and WAAM printed Ti-6Al-4V components, Mater. Des. 89 (2016) 559–567. doi:10.1016/j.matdes.2015.09.115.

[5] D. Ding, Z. Pan, D. Cuiuri, H. Li, Wire-feed additive manufacturing of metal components: technologies, developments and future interests, Int. J. Adv. Manuf. Technol. 81 (2015) 465–481. doi:10.1007/s00170-015-7077-3.

[6] J. Ding, P. Colegrove, J. Mehnen, S. Ganguly, P.M.S. Almeida, F. Wang, S. Williams, Thermo-mechanical analysis of Wire and Arc Additive Layer Manufacturing process on large multi-layer parts, Comput. Mater. Sci. 50 (2011) 3315–3322. doi:10.1016/j.commatsci.2011.06.023.

[7] H. Zhao, G. Zhang, Z. Yin, L. Wu, Effects of Interpass Idle Time on Thermal Stresses in Multipass Multilayer Weld-Based Rapid Prototyping, J. Manuf. Sci. Eng. 135 (2013) 11016. doi:10.1115/1.4023363.

[8] H. Geng, J. Li, J. Xiong, X. Lin, Optimisation of interpass temperature and heat input for wire and arc additive manufacturing 5A06 aluminium alloy, Sci. Technol. Weld. Join. 0 (2016) 1–12. doi:10.1080/13621718.2016.1259031.

[9] C. Shen, Z. Pan, D. Cuiuri, D. Ding, H. Li, Influences of deposition current and interpass temperature to the Fe3Al-based iron aluminide fabricated using wire-arc additive manufacturing process, Int. J. Adv. Manuf. Technol. 88 (2017) 2009–2018. doi:10.1007/s00170-016-8935-3.

[10] C. Shen, Z. Pan, Y. Ma, D. Cuiuri, H. Li, Fabrication of iron-rich Fe-Al intermetallics using the wire-arc additive manufacturing process, Addit. Manuf. 7 (2015) 20–26. doi:10.1016/j.addma.2015.06.001.

[11] Y. Ma, D. Cuiuri, C. Shen, H. Li, Z. Pan, Effect of interpass temperature on in-situ alloying and additive manufacturing of titanium aluminides using gas tungsten arc welding, Addit. Manuf. 8 (2015) 71–77. doi:10.1016/j.addma.2015.08.001.

[12] M.P. Mughal, H. Fawad, R. a Mufti, M. Siddique, Deformation modelling in layered manufacturing of metallic parts using gas metal arc welding: effect of process parameters, Model. Simul. Mater. Sci. Eng. 13 (2005) 1187–1204. doi:10.1088/0965-0393/13/7/013.

[13] H. Zhao, G. Zhang, Z. Yin, L. Wu, A 3D dynamic analysis of thermal behavior during single-pass multi-layer weld-based rapid prototyping, J. Mater. Process. Technol. 211 (2011) 488–495. doi:10.1016/j.jmatprotec.2010.11.002.

[14] J.F. Wang, Q.J. Sun, H. Wang, J.P. Liu, J.C. Feng, Effect of location on microstructure and mechanical properties of additive layer manufactured Inconel 625 using gas tungsten arc welding, Mater. Sci. Eng. A. 676 (2016) 395–405. doi:10.1016/j.msea.2016.09.015.

[15] K. Zhang, S. Wang, W. Liu, X. Shang, Characterization of stainless steel parts by Laser Metal Deposition Shaping, Mater. Des. 55 (2014) 104–119. doi:10.1016/j.matdes.2013.09.006.

[16] J.D. Spencer, P.M. Dickens, C.M. Wykes, Rapid prototyping of metal parts by three-dimensional welding, Proc. Inst. Mech. Eng. Part B J. Eng. Manuf. 212 (1998) 175–182. doi:10.1243/0954405981515590.

[17] X.P. Ding, H.M. Li, J.Q. Zhu, G.Y. Wang, H.Z. Cao, Q. Zhang, H.L. Ma, Application of infrared thermography for laser metal-wire additive manufacturing in vacuum, Infrared Phys. Technol. 81 (2017) 166–169. doi:10.1016/j.infrared.2016.12.017.

[18] J. Ding, P. Colegrove, J. Mehnen, S. Williams, F. Wang, P.S. Almeida, A computationally efficient finite element model of wire and arc additive manufacture, Int. J. Adv. Manuf.

Technol. 70 (2014) 227–236. doi:10.1007/s00170-013-5261-x.
[19] E.R. Denlinger, V. Jagdale, G. V Srinivasan, T. El-Wardany, P. Michaleris, Thermal modeling of Inconel 718 processed with powder bed fusion and experimental validation using in situ measurements, Addit. Manuf. 11 (2016) 7–15. doi:10.1016/j.addma.2016.03.003.
[20] X. Bai, H. Zhang, G. Wang, Improving prediction accuracy of thermal analysis for weld-based additive manufacturing by calibrating input parameters using IR imaging, Int. J. Adv. Manuf. Technol. 69 (2013) 1087–1095. doi:10.1007/s00170-013-5102-y.
[21] L. Parry, I.A. Ashcroft, R.D. Wildman, Understanding the effect of laser scan strategy on residual stress in selective laser melting through thermo-mechanical simulation, Addit. Manuf. 12 (2016) 1–15. doi:10.1016/j.addma.2016.05.014.
[22] F. Montevecchi, G. Venturini, A. Scippa, G. Campatelli, Finite Element Modelling of Wire-arc-additive-manufacturing Process, in: Procedia CIRP, 2016: pp. 109–114. doi:10.1016/j.procir.2016.08.024.
[23] F. Montevecchi, G. Venturini, N. Grossi, A. Scippa, G. Campatelli, Finite Element mesh coarsening for effective distortion prediction in Wire Arc Additive Manufacturing, Addit. Manuf. 18 (2017) 145–155. doi:10.1016/j.addma.2017.10.010.
[24] J. Hu, H.L. Tsai, Heat and mass transfer in gas metal arc welding. Part I: The arc, Int. J. Heat Mass Transf. 50 (2007) 833–846. doi:10.1016/j.ijheatmasstransfer.2006.08.025.
[25] J. Goldak, A. Chakravarti, M. Bibby, A new finite element model for welding heat sources, Metall. Trans. B. 15 (1984) 299–305. doi:10.1007/BF02667333.
[26] P. Michaleris, Modeling metal deposition in heat transfer analyses of additive manufacturing processes, Finite Elem. Anal. Des. 86 (2014) 51–60. doi:10.1016/j.finel.2014.04.003.
[27] P. Lindström, B. Josefson, M. Schill, T. Borrvall, Constitutive Modeling and Finite Element Simulation of Multi Pass Girth Welds, in: Proc. NAFEMS Nord. Conf., Gothernburg, 2012: pp. 22–23.
[28] J.O. Hallquist, LS-DYNA{®} Keyword User's Manual: Volumes I, II, and III LSDYNA R7. 1, 2014.
[29] EPRI, Carbon Steel Handbook, Palo Alto (CA), 2007. doi:1014670.
[30] P. Michaleris, a Debiccari, Prediction of welding distortion, Weld. J. Miami Fla. 76 (1997) 172–s. doi:10.1016/j.jmatprotec.2007.10.009.
[31] E.J. Soderstrom, K.M. Scott, P.F. Mendez, Calorimetric Measurement of Droplet Temperature in GMAW, Weld. J. 90 (2011) 77S–84S.
[32] T. Kargul, E. Wielgosz, J. Falkus, Application of Thermal Analysis Tests Results in the Numerical Simulations of Continuous Casting Process, Arch. Metall. Mater. 60 (2015). doi:10.1515/amm-2015-0035.
[33] F. Kreith, R.M. Manglik, M.S. Bohn, Principles of Heat Transfer, Cengage learning, Mason, OH, United States, 2010.
[34] H. Zhao, G. Zhang, Z. Yin, L. Wu, Three-dimensional finite element analysis of thermal stress in single-pass multi-layer weld-based rapid prototyping, J. Mater. Process. Technol. 212 (2012) 276–285. doi:10.1016/j.jmatprotec.2011.09.012.
[35] M. Hao, Y. Sun, A FEM model for simulating temperature field in coaxial laser cladding of TI6AL4V alloy using an inverse modeling approach, Int. J. Heat Mass Transf. 64 (2013) 352–360. doi:10.1016/j.ijheatmasstransfer.2013.04.050.
[36] P.A. Colegrove, H.E. Coules, J. Fairman, F. Martina, T. Kashoob, H. Mamash, L.D. Cozzolino, Microstructure and residual stress improvement in wire and arc additively manufactured parts through high-pressure rolling, J. Mater. Process. Technol. 213 (2013) 1782–1791. doi:10.1016/j.jmatprotec.2013.04.012.